



Published in final edited form as:

Biomech Model Mechanobiol. 2013 June ; 12(3): 467–474. doi:10.1007/s10237-012-0417-4.

Potential fluid mechanic pathways of platelet activation

Shawn C. Shadden and Sahar Hendabadi

Illinois Institute of Technology Chicago, IL, Tel.: +1-312-567-5126, Fax: +1-312-567-7230

Shawn C. Shadden: shawn.shadden@iit.edu

Abstract

Platelet activation is a precursor for blood clotting, which plays leading roles in many vascular complications and causes of death. Platelets can be activated by chemical or mechanical stimuli. Mechanically, platelet activation has been shown to be a function of elevated shear stress and exposure time. These contributions can be combined by considering the cumulative stress or strain on a platelet as it is transported. Here we develop a framework for computing a hemodynamic-based activation potential that is derived from a Lagrangian integral of strain rate magnitude. We demonstrate that such a measure is generally maximized along, and near to, distinguished material surfaces in the flow. The connections between activation potential and these structures are illustrated through stenotic flow computations. We uncover two distinct structures that may explain observed thrombus formation at the apex and downstream of stenoses. More broadly, these findings suggest fundamental relationships may exist between potential fluid mechanic pathways for mechanical platelet activation and the mechanisms governing their transport.

Keywords

clotting; hemodynamics; Lagrangian coherent structures; stenosis; thrombosis; transport

1 Introduction

As platelets are transported they are continuously stretched, compressed and sheared by local gradients in the flow. Exposure to elevated gradients can cause platelets to actively react with conformational, chemical and enzymatic responses, i.e. becoming activated. Once switched to the activated state, platelets perform multifaceted roles to orchestrate clotting. Here preliminary work related to the possible origins of mechanical activation, and relation to fundamental fluid mechanic structures, is discussed.

Mechanically-induced platelet activation under pathological conditions has been studied since the late 1970s. Colantuoni et al (1977) and Ramstack et al (1979) showed that platelet activation is a function of elevated shear rate and exposure time. Hellums (1994) developed a locus of platelet activation on a shear stress-exposure time plane that has been a standard for mechanical platelet activation threshold. Other studies have furthered understandings into mechanical platelet activation and its role in thrombosis, see e.g. recent studies of Nesbitt et al (2009); Rubenstein and Yin (2010); Sheriff et al (2010).

Most inferences between platelet activation and shear stress have been based on bulk quantities under uniform flow conditions. Experimental systems are typically devised to provide precise level of wall shear stress for a certain duration. While such experiments provide evidence of mechanical activation of platelets, the relevance of these findings must be translated to understanding more complex biomechanical processes occurring *in vivo*.

The stresses acting on a platelet change over space and time as the platelet is advected, and wall shear stress may only be marginally related to the stresses that platelets experience. Bluestein et al (1997) introduced a level of activation parameter for a platelet, defined as $\Sigma \bar{\tau} \times \Delta t$, where $\bar{\tau}$ is the average shear stress in a subset of a vessel (e.g. voxel of a discretized domain) and Δt is the exposure time of a platelet in that voxel. The sum is over all voxels the platelet passes through during a specified time interval. Other works have introduced similar trajectory-based activation models (Tambasco and Steinman, 2003; Alemu and Bluestein, 2007; Nobili et al, 2008). It is partly these works that we build on, and partly previous work of Shadden and Taylor (2008) describing coherent structures in cardiovascular flow.

Previous activation parameters have been defined from a component of the stress tensor (e.g. τ_{zz}), or an average of various components of the stress tensor (Alemu and Bluestein, 2007). Stress is a vector defined in terms of a reference plane. It is often not clear what reference plane should be used in a complex flow. In general, a platelet experiences a spectrum of elongation and shear stresses as it is transported, and the dominant components may change quickly and unpredictably. Here we introduce a new activation parameter. We consider a direction-independent measure of all independent deformation components. This measure is introduced as an activation potential in two senses. First, it provides a measure of mechanical strain, which has been shown to have the potential to activate platelets. Second, it is plotted at the initial location of the platelets. This latter condition is subtle, but it enables us to uncover an interesting observation that locations of highest activation potential tend to occur along structures that have important implications to the transport topology; this observation is the central point of this article.

2 Method

2.1 Activation potential

Herein blood is modeled as a fluid, and a platelet ($\approx 2 \mu\text{m}$ diameter) as a fluid element. While blood is more properly characterized as a suspension, due mainly to presence of red blood cells, modeling blood as a fluid is considered reasonable in vessels larger than 0.1 mm diameter (Cokelet, 1972). Indeed, it is typically in vessels with diameter > 1 mm where secondary flow structures develop that are hypothesized to influence platelet activation and aggregation. The features we seek to discuss result from fluid dynamics. Due to their scale and robustness, these structures likely persist through variations introduced by cellular interaction in the larger vessels for the moderate and higher strain rates shown to induce mechanical platelet activation.

From the fluid mechanic standpoint, the deformation of a platelet results from the symmetric portion of the velocity gradient, i.e. the rate of strain/deformation tensor

$$\mathbf{e}(\mathbf{x}, \mathbf{t}) = \frac{1}{2} \left[\partial_x \mathbf{u}(\mathbf{x}, \mathbf{t}) + \partial_x \mathbf{u}(\mathbf{x}, \mathbf{t})^T \right], \quad (1)$$

whereas the antisymmetric part, i.e. vorticity tensor

$$\mathbf{\Omega}(\mathbf{x}, \mathbf{t}) = \frac{1}{2} \left[\partial_x \mathbf{u}(\mathbf{x}, \mathbf{t}) - \partial_x \mathbf{u}(\mathbf{x}, \mathbf{t})^T \right], \quad (2)$$

is responsible for rotation.¹ The rate of deformation tensor is related to the local stress tensor in the fluid through a constitutive equation. The Newtonian approximation $\mathbf{s}(\mathbf{x}, t) = 2\mu\mathbf{e}(\mathbf{x}, t)$, where \mathbf{s} is the viscous stress tensor and μ is the kinematic viscosity, is considered reasonable

in blood flow where rates of deformation are sufficient to dominate cellular interaction, e.g. $\|\mathbf{e}\| > 100 \text{ s}^{-1}$ (Pedley, 1980). Depending on flow conditions, different viscosities, or constitutive models can be used (Cho and Kensey, 1991). While there is some uncertainty to the precise rheological properties of blood, force and deformation are monotonically related. Therefore, following normal convention, the roles of stress or strain rate can be viewed interchangeably, and the mechanical activation of platelets can be seen as originating from force or deformation. This view is consistent with hypotheses of mechanotransduction on cellular elements (Wang et al, 1993), where force-induced deformations result in cell signaling.

Wall shear stress (WSS) is predominantly used to identify “unfavorable” hemodynamic conditions. Several measurements have shown that platelet density increases near the wall for fully developed flows. However, for complex flow associated with medium to large vessels, especially those that are diseased, this assumption may break down. Platelet activation may occur over the entire domain, not just at the wall, and hence WSS may only be marginally related to platelet activation under disturbed flow conditions. Defining a shear stress, or any stress, at a platelet is not well-posed, since no obvious reference plane may exist. One could define a stress, or rate of deformation, distribution over the platelet surface, but consistent with our continuum assumption, we consider the magnitude of the total rate of deformation acting on a platelet.

We introduce an activation potential (AP) for a platelet at position $\mathbf{x}_0 = \mathbf{x}(t_0)$ at time t_0 as $\alpha(\mathbf{x}_0, t_0; t)$:

$$\alpha(\mathbf{x}_0, t_0; t) = \int_{t_0}^t \|\mathbf{e}(\mathbf{x}(\mathbf{s}), \mathbf{s})\|_F \, d, \quad (3)$$

where $\mathbf{x}(s)$ on the right hand side is evaluated along the platelet's trajectory. The integration time is considered a parameter. While several operator norms are possible, the Frobenius norm is chosen since this norm weighs each singular value of \mathbf{e} . That is,

$$\|\mathbf{e}\|_F = \sqrt{\text{tr}(\mathbf{e} \mathbf{e}^T)} \quad (4)$$

$$= \sqrt{\text{tr}(\mathbf{e}^2)} \quad (5)$$

$$= \sqrt{\sigma_1^2(\mathbf{e}) + \sigma_2^2(\mathbf{e}) + \sigma_3^2(\mathbf{e})}, \quad (6)$$

where $\sigma_i(\mathbf{e})$ are eigenvalues of \mathbf{e} . Thus all principal rates of deformation (and hence principal stresses) are considered in defining activation potential. Alternatively, it can be shown

$$\|\mathbf{e}\|_F = \sqrt{\sum_{i=1}^3 \sum_{j=1}^3 e_{ij}^2}. \quad (7)$$

¹Herein vector and tensor valued functions are set in bold face.

Since the diagonal entries of \mathbf{e} denote the 3 independent rates of linear deformation and the off diagonal entries denote the 3 independent rates of angular deformation, this definition represents a direction-independent measure of all independent deformation components, not just angular deformation or shear stress. This is motivated by previous experimental evidence that demonstrated platelet activation can occur from either tangential or normal stress (Purvis and Giorgio, 1991).

2.2 Relationship of AP to FTLE and LCS

If α is plotted at the initial location of the platelets then the activation potential is generally maximized along distinct material surfaces, otherwise known as repelling LCS (Lagrangian coherent structures), cf. §3. LCS have a rich background in dynamical systems theory and the study of fluid advection; see Shadden (2011) for a review. LCS are intrinsic objects that organize fluid advection patterns in wide-ranging laminar and turbulent flows. Heuristically, attracting/repelling LCS are defined as the locally most attracting/repelling material surfaces in the flow (Haller and Yuan, 2000). Thus, in addition to their role in organizing transport, we may expect the deformation of platelets along such material surfaces to be maximized, and hence their potential for activation.

Understanding the connection between AP and LCS more closely requires precise definition of LCS. Research into how LCS are best defined mathematically, or computed practically, in comparison to empirical evidence is ongoing. LCS are often computed as surfaces that locally maximize a finitetime Lyapunov exponent (FTLE) measure (Shadden et al, 2005; Lekien et al, 2007). The FTLE measures the maximum averaged logarithmic deformation rate of a fluid element over time. Since the FTLE is the de facto method to compute LCS, the relationship between the FTLE and the AP is derived in the Appendix.

Specifically, the FTLE, λ , is defined by considering the maximum deformation of a perturbation ξ from a trajectory $\mathbf{x}(t)$ from time t_0 to t , i.e.

$$\lambda(x_0, t_0; t) = \frac{1}{|t - t_0|} \ln \max_{\xi_0} \frac{\|\xi_t\|}{\|\xi_0\|}. \quad (8)$$

As shown in the Appendix,

$$\frac{\|\xi_t\|}{\|\xi_0\|} = \int_{t_0}^t \left[\hat{\xi}_t \cdot \mathbf{e}(x, \mathbf{s}) \hat{\xi}_0 - \mathbf{0.5} \|\omega(x, \mathbf{s})\| \cos\phi \sin\psi \right] ds + \cos\psi, \quad (9)$$

where ω is the vorticity vector and the angles ϕ and ψ are defined therein. From Eq. (9) it is clear that the FTLE depends on more than just the magnitude of the rate of deformation tensor \mathbf{e} . Even in the absence of vorticity,

$$\frac{\|\xi_t\|}{\|\xi_0\|} = \int_{t_0}^t \left[\hat{\xi}_t \cdot \mathbf{e}(x, \mathbf{s}) \hat{\xi}_0 \right] ds + \cos\psi, \quad (10)$$

the FTLE depends on how the rate of deformation tensor rotates line elements. In the computation of the AP, all rotational information is essentially discarded since the magnitude of the rate of deformation tensor is accrued at each time step of the integration. In the computation of the FTLE however, the deformation magnitude is computed not at each step, but at the end of the integration interval, whereby rotation of the strain rate eigenvectors may contribute to the measured deformation magnitude.

Continuous deformation, even if resulting in zero or little net deformation, can induce mechanotransduction. Therefore the computation of integrated deformation in Eq. (3) is preferred to the deformation measure in Eq. (8) for the purpose of studying mechanically-induced platelet activation. However, even though the FTLE and AP are distinct quantities, both tend to be locally maximized along LCS, as shown below. Indeed, various methods to identify LCS exist since no single definition has proven satisfactory over the vast spectrum of complexity encountered in fluid flow. Although the spatial distribution of the FTLE is usually accurate and robust, other related “stretching measures” are known to be more or less effective in identifying similar structures (Aurell et al, 1997; Lapeyre et al, 2001). The important observation herein is that LCS tend to locally maximize mechanical strain hypothesized to affect platelet activation, which we will demonstrate next through stenotic flow data.

3 Results

Stenotic flow conditions are important to thrombosis, especially in the coronary arteries. A simplified model of a coronary stenosis (Fig. 1) was used for demonstration of the AP computation. The native vessel diameter and volumetric flow data were based on canine left anterior descending (LAD) artery data from LaDisa et al (2002). The stenosis geometry, originally from Young and Tsai (1973), has been used extensively in previous studies and corresponds to an area reduction of 82.5%.

A computer model was constructed using a customized version of SimVascular (Schmidt et al, 2008). The model was discretized into approximately 2.74 million tetrahedral elements with nominal edge size $100\ \mu\text{m}$. This edge size is close to the Kolmogorov microscale, although no turbulence was observed. The flow waveform in Fig. 1 was mapped to a Poiseuille cross-sectional profile and imposed at the inlet, which was 5 diameters from the start of the stenosis. A resistance boundary condition was imposed at the outlet with resistance $R = 18.19\ \text{g}\ \text{mm}^{-4}\ \text{s}^{-1}$, calculated from $\bar{p} = \bar{Q}R$ using the mean flow rate \bar{Q} from the inflow waveform and a mean physiologic blood pressure \bar{p} of 100 mmHg. A no slip condition was imposed on the vessel wall.

Blood was modeled as an incompressible, Newtonian fluid ($\rho = 1.06\ \text{g}\ \text{cm}^{-3}$, $\mu = 0.04\ \text{g}\ \text{cm}^{-1}\ \text{s}^{-1}$). The Navier Stokes equations were solved using a second-order accurate, stabilized finite element method based on works of Shakib et al (1989); Taylor et al (1998); Jansen et al (2000) and others, which has been used and validated extensively for hemodynamic simulations. The simulation time step size of $1.3 \times 10^{-4}\ \text{s}$ was based on $\text{CFL} < 1$. Six cardiac cycles were computed to ensure convergence, and the last three cycles were used for analysis. The peak Reynolds number at the inlet (based on the average velocity over the inlet at peak flow rate) was $Re_{df} = 142$, and similarly the Reynolds number during peak flow at the stenotic throat was $Re_{ds} = 340$.

Previous studies using the stenosis in Fig. 1 have primarily been restricted to 2D. The model used herein was constructed manually. This produced slight geometrical asymmetries resulting in a flow field that was 3D, which is more consistent with physiologic conditions than a perfectly symmetric vessel. Moreover, this distinction is important since some methods or phenomena in 2D flow analysis or topology cannot be easily extended or observed in 3D. In addition, unlike previous studies, a physiologic pulsatile flow wave was prescribed since the introduction of unsteadiness to the velocity field is also a defining characteristic in how the flow topology should be studied. That is, Eulerian methods used previously are most appropriate for understanding the transport topology under steady conditions, but can be inadequate otherwise.

Velocity data at four instances in a cardiac cycle are shown in Fig. 2. A core jet is observed through the stenotic throat that extends several diameters distally and is surrounded by regions of recirculation. At these times, the strain rate fields are also shown. High rates of strain are confined to the proximal wall of the stenosis and the shear layer between the fluid jet and the recirculation zone in the separated region. Maximum strain rates reaching $10,000 \text{ s}^{-1}$ were highly localized to the stenotic throat; a reduced color range was used however to aid visualization of elevated values.

The activation potential field was calculated from the flow data and the results at several instances during the cardiac cycle are shown in Figure 3. Due to the difficulty in visualizing the full 3D field, and the fine scale of the Lagrangian structures present, an arbitrary longitudinal cross-section of the AP field is shown so that the region in proximity to the stenosis could be better visualized. High values of AP are mostly localized along distinct surfaces (curves in the cross-sectional view). Upon close inspection of the fields, there is a persistent proximal structure of high AP that terminates near the apex of the stenosis, and a more wide ranging structure that terminates distal to the stenosis. These two structures are more easily distinguished from the AP field of a 2D simulation, where all geometrical parameters and boundary conditions were equivalent to the 3D simulation, as shown in the top row of Fig. 4. The values of AP along the proximal structure were generally higher than along the distal structure. The distal structure behaves as a “heteroclinic manifold” that entrains fluid into the recirculation region (Shadden et al, 2006). The proximal structure is dominated by shear, but also exhibits a separatrix nature, separating fluid that accumulates at the apex of the stenosis from that flushed downstream, as shown in the bottom row of Fig. 4.

Due to the asymmetry of the flow, the cross-sections shown in Figs. 3 and 4 may not exactly transverse maximal AP surfaces, i.e. LCS. The more tangent the cross-section is to the structure, the thicker the structure may appear. This may be most apparent in the recirculation region distal to the stenosis where azimuthal velocities become non-negligible. In addition, from Fig. 4 it is clear that more mixing and complexity of the flow is encountered in 3D than 2D, as might be expected.

4 Discussion

From Fig. 2, the maximum values of strain rate occur along the proximal wall of the stenosis, at the throat, and the shear layer between the fluid jet and recirculation region. The strain rate values observed in these regions range from $1,000 - 10,000 \text{ s}^{-1}$; these levels are in the range considered sufficient for platelet activation (Hellums, 1994). Although the strain rate, or similar Eulerian fields, are widely used to characterize flow conditions, it is difficult to assess what happens to platelets passing through high strain rate regions by visualizing snapshots of instantaneous Eulerian information. Specifically, one is compelled to question whether such platelets are immediately advected downstream, or tend to become entrained into the recirculation zone; either situation could have distinct consequences to the development of mural thrombus. To understand the accumulated strain on each fluid element as it is advected, the AP computation in Eq. (3) is performed. This measure helps to determine the platelets most likely to become activated by mechanical means. Interestingly, high values of AP coincide with distinct material surfaces. Notably, the distribution of AP is organized by fundamental features in the flow that also organize the transport topology. This observation helps uncover what happens to these platelets as they are transported, which is discussed next. It is important to keep in mind that since AP is plotted at the initial particle locations, high AP corresponds to particles that will subsequently experience the highest integrated strain.

The distal structure highlighted in Fig. 4 can be considered an attachment profile, or a boundary between the fluid that recirculates from that continuing downstream. Tracing this curve from right to left (upstream), it loops progressively back and forth. Proximal to the stenosis, this looping traces out lobes of fluid in the near-wall region where elevated strain rate is observed. These lobes contain precisely the fluid that is entrained into the recirculation region downstream of the stenosis. On the downstream side, the structure forms bounded lobes. This occurs because the LCS is a material surface and therefore cannot self-intersect. Therefore lobes on the distal side of the stenosis become confined by previous segments of the structure, see e.g. the curling of the bounded segment of the distal structure in the top right of Fig. 4. This bounding of the structure creates a region of high AP distal to the stenosis, which may promote platelet aggregation. Specifically, these features may help explain the biomechanics underlying observations of thrombosis downstream of stenoses (Nesbitt et al, 2009), which are currently based on a hypothesis of a “shear gradient” mechanism, which ignores important transport processes that are uncovered here. We observe that platelets with elevated AP tend to be entrained into the recirculation region, than advected downstream. This may significantly increase the likelihood of aggregation in the downstream region. It is important to point out that platelets can be detrained from the recirculation region. To understand detraining, one must also compute *attracting* LCS, cf. Shadden et al (2007).

The proximal structure revealed in the AP plots, and highlighted in Fig. 4, has generally higher AP values than the distal structure and is primarily shear dominated. This structure is located approximately 80–100 μm away from the wall, which is large compared to the size of a platelet. Therefore maximum integrated shearing occurs on platelets away from the wall. Interestingly, this structure has an accumulation point near the apex of the stenosis, which may explain why thrombus also routinely forms at this location (Barstad et al, 1994). The current hypothesis is that thrombus forms here because it is where instantaneous strain rate is maximized. However, we reveal that the influence may propagate well upstream.

For the proximal and distal structures discussed above, the importance and interrelation of fluid transport *and* hemodynamic forcing to observed locations of platelet aggregation is clearly revealed using this approach. These mechanistic understandings into the transport of potentially activated platelets would be difficult to assess without uncovering the relationships to LCS. For example, direct analysis of transport would entail computing and visualizing the trajectories of a distribution of particles. Each particle could be color-coded over time according to its level of activation potential to better understand where potentially activated platelets are transported. However, this would present at least two main challenges. First, unlike streamlines, pathlines are typically chaotic and convoluted making it difficult to accurately or precisely infer the flow topology. This is why such plots are rarely presented to quantify flow physics. Second, the vast majority of the particles are quickly flushed from the domain. To track these, the domain would have to be arbitrarily extended downstream to determine definitively where the particles with highest AP end up. While awkward from a practical standpoint, this is also questionable in more realistic, subject-specific geometries because vessels branch, bend, taper, etcetera *in vivo* and cannot be extended arbitrarily without biasing the results.

The framework presented here enables understandings into how localized changes in morphology influence inherently non-local (in space and time) fluid mechanical phenomena. Namely, this occurs by plotting the AP at the initial particle locations, since this results in a structured distribution that is analogous to an Eulerian field. This is advantageous because the field is easily visualized compared to a chaotic distribution of paths. However, this method retains critical insight into the true unsteady dynamics. This is because high AP

localizes to fundamental material surfaces that behave as separatrices partitioning regions of flow with distinct Lagrangian dynamics.

One should keep in mind that platelet activation is not well-defined or completely understood. Hence, measures for AP as presented here are most appropriately considered a potential for activation in a broad sense. For example, a platelet with high AP could be viewed as potentially susceptible to chemical activation if not fully “activated” by mechanical influence. This is particularly important in situations where thrombus, or a legion, already exists and chemical agonists are locally present; or locations where a concentration of activated platelets exists, since activated platelets release factors that activate nearby quiescent platelets.

4.1 Limitations

The definition of AP presented here is a first order approximation. Evidence suggests that mechanical activation depends on the level of strain rate platelets are exposed to, and the exposure time. While these dependencies are likely monotonic, it is unclear over what conditions they can be considered linear. Nonlinear relationships have also been proposed, see e.g. Tambasco and Steinman (2003); Borenda et al (1995); Alemu and Bluestein (2007); Nobili et al (2008). Regardless, it is reasonable to expect both linear and nonlinear relationships to be locally maximized along LCS. The reasons for this are (1) that LCS are locally the most repelling surfaces in the flow, often “exponentially” more repelling than other surfaces, a property that is leveraged to effectively compute them. Most measures monotonically dependent on deformation will tend to be maximized in this regard along such surfaces. And (2) LCS persist over time since they are based on finite time averages, than from instantaneous information normally used to classify flow, and likewise would imply persistent exposure.

Another limitation is the assumption that a platelet can be modeled as a fluid element. Modeling a platelet as a rigid spherical particle with finite size and unique density is relatively straightforward using e.g. the equations described by Maxey and Riley (1983). This was implemented for the computations herein and resulted in practically indistinguishable results for particles sized 2–10 microns. However, realistic modeling of the interactions of platelets with each other, or with the vessel wall, is exceedingly complex, even in the absence of chemical or enzymatic reactions. Very close to the wall, or in low flow regions containing activated platelets, a platelet is likely to adhere, or cohere, respectively. Accurate modeling of platelet adhesion and cohesion under physiologic flows on this scale in whole blood is an active area of research and for the most part remains intractable. While appropriate modifications could be made as modeling improves, the time scales of platelet aggregation (tens of seconds to minutes) are generally longer than the time scales of the mechanisms described herein.

4.2 Conclusion

Blood flow influences biology by way of forces and by way of transport. Traditionally these influences have been considered separately, although transport processes have received less attention. The results herein indicate potential synergistic relationships between the kinematic mechanisms underlying transport, and the dynamic mechanisms underlying mechanical platelet activation. The methods presented enable such findings to be explored, providing a framework to better handle the complex mechanisms that can occur *in vivo*.

Appendix

Consider a platelet centered around trajectory $\mathbf{x}(\mathbf{x}_0, t_0, t)$ starting at \mathbf{x}_0 at time t_0 , and an arbitrary surface point $\mathbf{y}(\mathbf{y}_0, t_0, t) = \mathbf{x}(\mathbf{x}_0, t_0, t) + \xi_t$. By linearization of $\mathbf{x}(\mathbf{x}_0, t_0, t)$

$$\xi_t = \partial_{x_0} \mathbf{x}(\mathbf{x}_0, \mathbf{t}_0, \mathbf{t}) \xi_0, \quad (11)$$

which holds for $\|\xi_0\|$ sufficiently small. The magnitude squared gives

$$\|\xi_t\|^2 = \xi_0^T \partial_{x_0} \mathbf{x}(\mathbf{x}_0, \mathbf{t}_0, \mathbf{t})^T \partial_{x_0} \mathbf{x}(\mathbf{x}_0, \mathbf{t}_0, \mathbf{t}) \xi_0. \quad (12)$$

The (largest) FTLE is associated with measuring maximal deformation ξ_t . From Eq. (12), this occurs when ξ_0 is parallel to the eigenvector of the maximum eigenvalue of

$$\Delta(\mathbf{x}_0, t_0, t) = \partial_{x_0} \mathbf{x}(\mathbf{x}_0, \mathbf{t}_0, \mathbf{t})^T \partial_{x_0} \mathbf{x}(\mathbf{x}_0, \mathbf{t}_0, \mathbf{t}).$$

Letting $\chi(\mathbf{x}_0, t_0, t)$ denote this largest eigenvalue, the maximum stretching factor is

$$\max_{\xi_0} \frac{\|\xi_t\|}{\|\xi_0\|} = \sqrt{\chi(\mathbf{x}_0, t_0, t)} = \|\partial_{x_0} \mathbf{x}(\mathbf{x}_0, \mathbf{t}_0, \mathbf{t})\|_2, \quad (13)$$

where $\|\cdot\|_2$ denotes the matrix norm induced from the standard vector norm. The FTLE is defined by taking the natural logarithm and dividing by the integration time, i.e.

$$\lambda(\mathbf{x}_0, t_0; t) = \frac{1}{|t - t_0|} \ln \max_{\xi_0} \frac{\|\xi_t\|}{\|\xi_0\|}. \quad (14)$$

To compare with AP, the contribution of integrated strain rate to the growth of ξ_t is considered. The evolution of $\mathbf{x}(\mathbf{x}_0, t_0, t)$ is governed by the advection equation

$$\partial_t \mathbf{x}(\mathbf{x}_0, \mathbf{t}_0, \mathbf{t}) = \mathbf{u}(\mathbf{x}, \mathbf{t}), \quad (15)$$

where \mathbf{u} is the fluid velocity. Linearizing Eq. (15) about $\mathbf{x}(\mathbf{x}_0, t_0, t)$ gives

$$\partial_t \xi_t = \partial_x \mathbf{u}(\mathbf{x}, \mathbf{t}) \xi_0. \quad (16)$$

The velocity gradient can be written as the sum of \mathbf{e} and $\mathbf{\Omega}$, hence

$$\partial_t \xi_t = \mathbf{e}(\mathbf{x}, \mathbf{t}) \xi_0 + \mathbf{\Omega}(\mathbf{x}, \mathbf{t}) \xi_0. \quad (17)$$

The vorticity tensor has 3 independent components and can be written in vector form as $\boldsymbol{\omega} = \nabla \times \mathbf{u}$, so that $\mathbf{\Omega} \xi_0 = \frac{1}{2} \boldsymbol{\omega} \times \xi_0$. Therefore

$$\partial_t \xi_t = \mathbf{e}(\mathbf{x}, \mathbf{t}) \xi_0 + \frac{1}{2} \boldsymbol{\omega}(\mathbf{x}, \mathbf{t}) \times \xi_0. \quad (18)$$

Integrating gives

$$\xi_t - \xi_0 = \int_{t_0}^t [e(x, s)\xi_0 + \mathbf{0.5}\omega(x, s) \times \xi_0] ds. \quad (19)$$

Dotting ξ_t with both sides gives

$$\xi_t \cdot \xi_t - \xi_t \cdot \xi_0 = \int_{t_0}^t [\xi_t \cdot e(x, s)\xi_0 + \mathbf{0.5}\xi_t \cdot \omega(x, s) \times \xi_0] ds. \quad (20)$$

Defining ϕ as the angle between ω and $\xi_t \times \xi_0$ and ψ is the angle between ξ_t and ξ_0 ,

$$\frac{\|\xi_t\|}{\|\xi_0\|} = \int_{t_0}^t \left[\hat{\xi}_t \cdot e(x, s)\hat{\xi}_0 - \mathbf{0.5}\|\omega(x, s)\|\cos\phi\sin\psi \right] ds + \cos\psi, \quad (21)$$

where the hat implies unit vector.

References

- Alemu Y, Bluestein D. Flow-induced platelet activation and damage accumulation in a mechanical heart valve: Numerical studies. *Artificial Organs*. 2007; 31(9):677–688. [PubMed: 17725695]
- Aurell E, Boffetta G, Crisanti A, Paladin G, Vulpiani A. Predictability in the large: an extension of the concept of Lyapunov exponent. *J Phys A*. 1997; 30(1):1–26.
- Barstad RM, Roald HE, Cui Y, Turitto VT, Sakariassen KS. A perfusion chamber developed to investigate thrombus formation and shear profiles in flowing native human blood at the apex of well-defined stenoses. *Arterioscler Thromb Vasc Biol*. 1994; 14(12):1984–1991.
- Bluestein D, Niu L, Schoepfoerster R, Dewanjee M. Fluid mechanics of arterial stenosis: Relationship to the development of mural thrombus. *Ann Biomed Eng*. 1997; 25(2):344–356. [PubMed: 9084839]
- Boreda R, Fatemi RS, Rittgers SE. Potential for platelet stimulation in critically stenosed carotid and coronary arteries. *J Vasc Invest*. 1995; 1(1):26–37.
- Cho YI, Kensey R. Effects of the non-Newtonian viscosity of blood flows in a diseased arterial vessel. Part 1: Steady flows. *Biorheology*. 1991; 28:241–262. [PubMed: 1932716]
- Cokelet, GR. The rheology of human blood. In: Fung, YC.; Perrone, N.; Anliker, M., editors. *Biomechanics: Its Foundations and Objectives*. Prentice-Hall: 1972. p. 63-103.
- Colantuoni G, Hellums JD, Moake JL, Alfrey CP. The response of human platelets to shear stress at short exposure times. *T Am Soc Art Int Org*. 1977; 23:626–631.
- Haller G, Yuan G. Lagrangian coherent structures and mixing in two-dimensional turbulence. *Physica D-Nonlinear Phenomena*. 2000; 147(3-4):352–370.
- Hellums JD. 1993 Whitaker lecture - Biorheology in thrombosis research. *Ann Biomed Eng*. 1994; 22(5):445–455. [PubMed: 7825747]
- Jansen KE, Whiting CH, Hulbert GM. A generalized- α method for integrating the filtered Navier-Stokes equations with a stabilized finite element method. *Comput Method Appl M*. 2000; 190(3-4):305–319.
- LaDisa JF, Hettrick DA, Olson LE, Guler I, Gross ER, Kress TT, Kersten JR, Warltier DC, Pagel PS. Stent implantation alters coronary artery hemodynamics and wall shear stress during maximal vasodilation. *J Appl Phys*. 2002; 93(6):1939–1946.
- Lapeyre G, Hua BL, Legras B. Comment on “Finding finite-time invariant manifolds in two-dimensional velocity fields”. *CHAOS*. 2001; 11(2):427–430. [Chaos 10, 99, (2000)]. [PubMed: 12779478]
- Lekien F, Shadden SC, Marsden JE. Lagrangian coherent structures in n-dimensional systems. *Journal of Mathematical Physics*. 2007; 48(6):065, 404–19.

- Maxey MR, Riley JJ. Equation of motion for a small rigid sphere in a nonuniform flow. *Phys Fluids*. 1983; 26:883–889.
- Nesbitt WS, Westin E, Tovar-Lopez FJ, Tolouei E, Mitchell A, Fu J, Carberry J, Fouras A, Jackson SP. A shear gradient-dependent platelet aggregation mechanism drives thrombus formation. *Nat Med*. 2009; 15(6):665–673. [PubMed: 19465929]
- Nobili M, Sheriff J, Morbiducci U, Redaelli A, Bluestein D. Platelet activation due to hemodynamic shear stresses: Damage accumulation model and comparison to in vitro measurements. *American Society for Artificial Internal Organs Journal*. 2008; 54(1):64–72.
- Pedley, TJ. *The Fluid Mechanics of Large Blood Vessels*. Cambridge University Press; 1980.
- Purvis NB, Giorgio TD. The effect of elongational stress exposure on the activation and aggregation of blood-platelets. *Biorheology*. 1991; 28(5):355–367. [PubMed: 1782391]
- Ramstack JM, Zuckerman L, Mockros LF. Shear-induced activation of platelets. *J Biomech*. 1979; 12(2):113–25. [PubMed: 422576]
- Rubenstein D, Yin W. Quantifying the effects of shear stress and shear exposure duration regulation on flow induced platelet activation and aggregation. *J Thromb Thrombolys*. 2010; 30(1):36–45.
- Schmidt JP, Delp SL, Sherman MA, Taylor CA, Pande VS, Altman RB. The simbios national center: Systems biology in motion. *Proceedings of the IEEE*. 2008; 96(8):1266–1280. [PubMed: 20107615]
- Shadden S, Katija K, Rosenfeld M, Marsden J, Dabiri J. Transport and stirring induced by vortex formation. *Journal of Fluid Mechanics*. 2007; 593:315–332.
- Shadden, SC. *Lagrangian Coherent Structures*. Wiley-VCH Verlag GmbH & Co; KGaA: 2011. p. 59–89.
- Shadden SC, Taylor CA. Characterization of coherent structures in the cardiovascular system. *Ann Biomed Eng*. 2008; 36(7):1152–1162. [PubMed: 18437573]
- Shadden SC, Lekien F, Marsden JE. Definition and properties of Lagrangian coherent structures from finite-time Lyapunov exponents in two-dimensional aperiodic flows. *Physica D*. 2005; 212(3–4): 271–304.
- Shadden SC, Dabiri JO, Marsden JE. Lagrangian analysis of fluid transport in empirical vortex ring flows. *Phys Fluids*. 2006; 18(4)
- Shakib F, Hughes TJR, Johan Z. A multi-element group preconditioned GMRES algorithm for nonsymmetric systems arising in finite-element analysis. *Computer Methods in Applied Mechanics and Engineering*. 1989; 75(1-3):415–456.
- Sheriff J, Bluestein D, Girdhar G, Jesty J. High-shear stress sensitizes platelets to subsequent low-shear conditions. *Ann Biomed Eng*. 2010; 38(4):1442–1450. [PubMed: 20135353]
- Tambasco M, Steinman DA. Path-dependent hemodynamics of the stenosed carotid bifurcation. *Annals of Biomedical Engineering*. 2003; 31(9):1054–1065. [PubMed: 14582608]
- Taylor CA, Hughes TJR, Zarins CK. Finite element modeling of blood flow in arteries. *Comput Method Appl M*. 1998; 158(1-2):155–196.
- Wang N, Butler JP, Ingber DE. Mechanotransduction across the cell surface and through the cytoskeleton. *Science*. 1993; 260:1124–1127. [PubMed: 7684161]
- Young D, Tsai F. Flow characteristics in models of arterial stenosis–I. Steady flow. *J Biomech*. 1973; 6(4):395–402. [PubMed: 4732939]

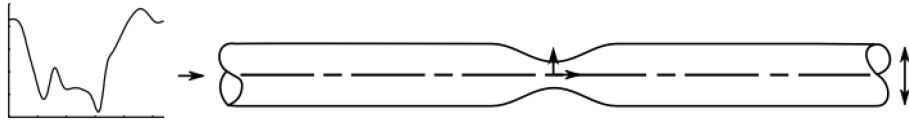


Fig. 1.
Stenosis profile and physiologic volumetric inflow waveform.

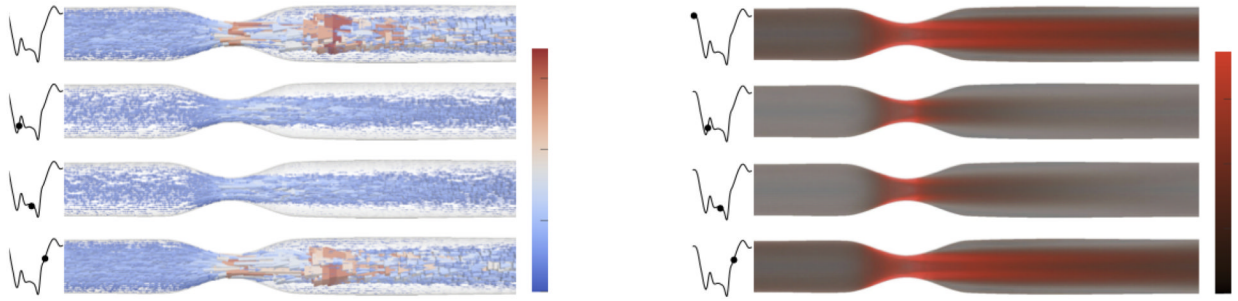


Fig. 2. Velocity (left) and strain rate (right) fields at equally-spaced times in the cycle. Velocity vectors are shown at a random sampling ($< 1\%$) of the nodes.

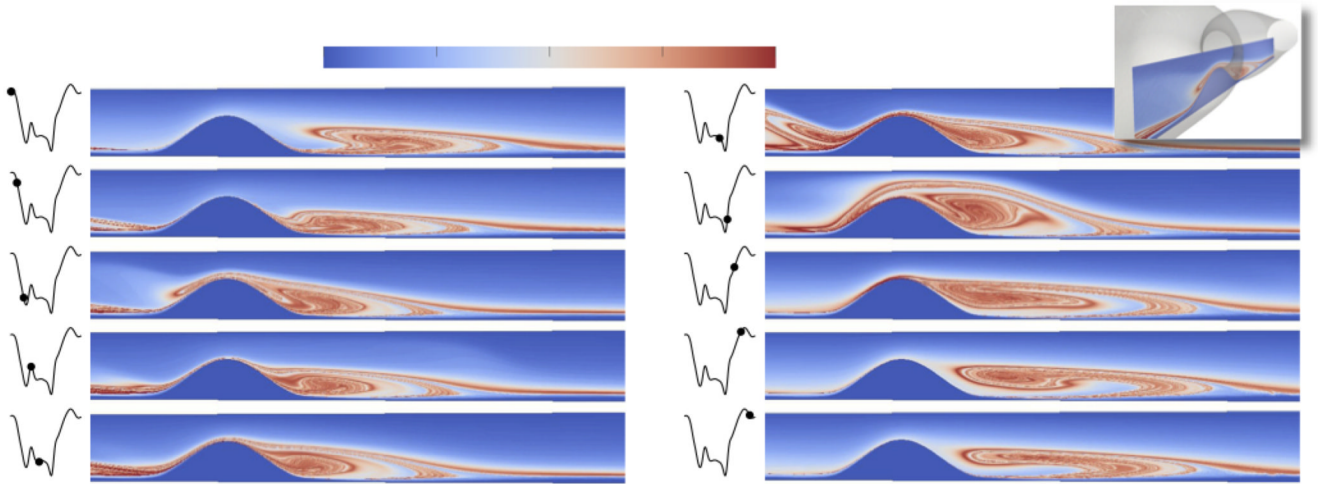


Fig. 3. Cross-section of the activation potential field near the stenosis. Location in reference to vessel is shown upper-right and vertical axis in each plot is scaled $\times 2$.

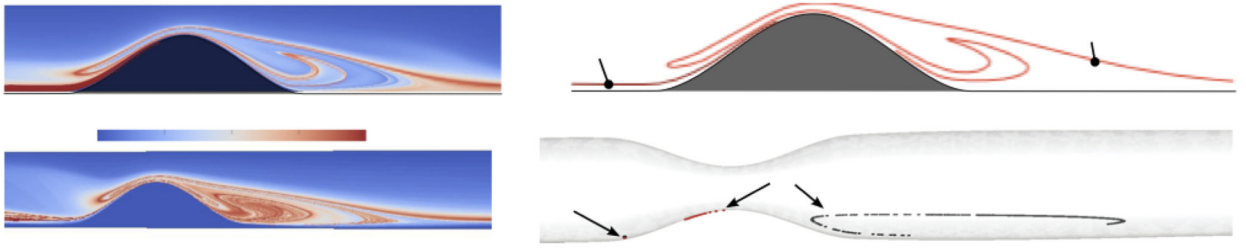


Fig. 4.

AP field for a 2D simulation (top left) and extracted structures (top right). The proximal structure is dominated by shear but also separates flow that accumulates near the apex, as shown for the 3D simulation in the bottom row. The starting locations of two groupings of particles (appearing as one point due to their proximity) are initially divided by the proximal structure in 3D AP field (bottom left). The later locations are plotted after 1 cardiac cycle of time had elapsed.